# Anti-Corrosion Methods and Materials

Sulfide stress cracking assessment of low-alloy L80 casing steel in $H_2S$ environment

Weishan Huang, Jing-Li Luo, Hani Henein, Josiah Jordan,

## Article information:

# Sulfide stress cracking assessment of low-alloy L80 casing steel in $H_2S$ environment

*Weishan Huang, Jing-Li Luo and Hani Henein*
Department of Chemical and Materials Engineering, University of Alberta, Edmonton, Canada, and
*Josiah Jordan*
Evraz Inc. NA, Regina, Canada

**Abstract**

**Purpose** – This paper aims to evaluate the sulfide stress cracking (SSC) resistance of L80 casing steels with different alloying chemistries (e.g. Ti-B and Mn-Cr-Mo) by correlating the reduction in area ratio with the mechanical property, inclusion and carbide.

**Design/methodology/approach** – SSC tests were conducted in 5.0 Wt.% sodium chloride and 0.5 Wt.% acetic acid solution saturated with $H_2S$ using constant load tensile method. The microstructure and fracture morphology of the steel were observed using scanning electron microscope. The inclusion and carbide were identified by energy dispersive spectroscopy and auger electron microscope.

**Findings** – Among all the testing steels, electric resistance welding (ERW) L80-0.5Mo steel demonstrates the highest SSC resistance because of its appropriate mechanical properties, uniform microstructure and low inclusion content. The SSC resistance of L80 steels generally decreases with the rising yield strength. The fracture mode of steel with low SSC resistance is jointly dominated by transgranular and intergranular cracking, whereas that with high SSC resistance is mainly transgranular cracking. SSC is more sensitive to inclusions than carbides because the cracks are easier to be initiated from the elongated inclusions and oversized oxide inclusions, especially the inclusion clusters. Unlike the elongated carbide, globular carbide in the steel can reduce the negative effect on the SSC resistance. Especially, a uniform microstructure with fine globular carbides favors a significant improvement in SSC resistance through precluding the cracking propagation.

**Originality/value** – The paper provides the new insights into the improvement in SSC resistance of L80 casing steel for its application in $H_2S$ environment through optimizing its alloying compositions and microstructure.

**Keywords** Sulfide stress cracking, Fracture mode, Inclusion, Carbide, L80 casing steel

**Paper type** Research paper



## 1. Introduction

In recent years, the growing energy demand has stimulated the active exploitation of an increasing number of sour oil and gas fields containing $H_2S$ (Choi *et al.*, 2011; Zheng *et al.*, 2014). Nowadays, more than one-third of worldwide oil and gas fields contain $H_2S$ (Sui *et al.*, 2017). For example, the extensively developed oil and gas wells in Western Canada have significant concentrations of $H_2S$. In this regard, the potential corrosion problems of carbon steel casing induced by $H_2S$ have been more frequently encountered in the drilling and exploitation environments (He *et al.*, 2009; Zhang *et al.*, 2012; Ding *et al.*, 2014).

It is well known that apart from the severe electrochemical corrosion, the most prominent problems for the casing steel in $H_2S$-containing environment are the environmental crackings such as sulfide stress cracking (SSC) and hydrogen-induced cracking (HIC) (Zhou *et al.*, 2013; Bai *et al.*, 2015; Lei *et al.*, 2018). SSC is usually generated from the steel surface under the applied stress. Its essence is a hydrogen embrittlement phenomenon which causes the steel failure below its yield strength. When hydrogen is cathodically evolved on the steel surface, the recombination of hydrogen atoms to form hydrogen molecules is greatly inhibited because of the poisoning effect of $H_2S$, which makes it easier for the hydrogen atoms to enter the steel. In the steel, the hydrogen atoms diffuse to the regions of high tri-axial stress or some microstructural sites (e.g. inclusions, grain boundaries and vacancies) where they are trapped and reduce the ductility of carbon steel (Peñalva *et al.*, 2012; Zhou *et al.*, 2013; Lei *et al.*, 2018). Despite of the high corrosion risk, carbon steel or low-alloy steel is still the cost-effective materials used for casing and tubing (Choi *et al.*, 2011; Sun *et al.*, 2018). So far, great efforts have been made to improve the corrosion resistance of carbon steel (López, *et al.*, 2003; Guo *et al.*, 2012; Wu *et al.*, 2013; Sun *et al.*, 2016), and alloying of carbon steel appears to be an effective way to improve the mechanical and structural properties of carbon steel, mitigating the SSC risk of carbon steel. Thus, it is critical to develop the alloying carbon steel, as

The current issue and full text archive of this journal is available on Emerald Insight at: **www.emeraldinsight.com/0003-5599.htm**

Anti-Corrosion Methods and Materials

[DOI 10.1108/ACMM-08-2018-1984]

This work is supported by Natural Sciences and Engineering Research Council of Canada and EVRAZ Inc. NA.

Received 9 August 2018
Revised 27 November 2018
Accepted 10 December 2018

it holds promise to compromise between the corrosion resistance and the associated costs.

Extensive studies on the effects of cleanliness and microstructures on the SSC resistance of steel (Golovanenko *et al.*, 1978; Koh *et al.*, 2004; Al-Mansour *et al.*, 2009; Beidokhti *et al.*, 2009; Jin et *al.*, 2010; Kang *et al.*, 2012) have suggested that the SSC initiation is usually associated with steel cleanliness. Elongated MnS inclusions and coarse cubic TiN particles are known to be the most detrimental initiation sites (Elboujdaini, 2011). The effect of microstructure on SSC resistance has been investigated for acicular ferrite, ferrite–pearlite, upper bainite/lower bainite, quenched and tempered martensite. It is found that the microstructure of ferrite and pearlite is the worst structure (Venegas *et al.*, 2005), whereas that of quenched and tempered martensite performs the best in sour environment (Sponseller *et al.*, 1983). Nevertheless, the relative importance of steel cleanliness and microstructure has not been elucidated. Also for low alloy steels, the role of alloying elements on varying the microstructure of these steels and its subsequent effect on SSC resistance still remains unclear.

The objective of this study is to investigate the SSC behavior of low-alloy L80 casing steels with different alloying chemistries (e.g. Ti-B and Mn-Cr-Mo) in $H_2S$ environment. The effects of microstructure, mechanical properties, inclusions and carbides on the SSC susceptibility of steel were investigated using constant load tensile method and surface analysis techniques. Accordingly, the dominant reason and factor for SSC performance are discussed to further understand the degradation of casing steel caused by $H_2S$. The findings provided herein form the base to technically support the option of using alloying strategy to improve the SSC resistance of carbon steel and promote its application in the $H_2S$ environment.

## 2. Experimental procedure

### 2.1 Materials

Six different low-alloy L80 casing steels, produced by Evraz Inc. NA, were used in this study. Their chemical compositions are listed in Table I. Electric arc furnace steelmaking process was used to produce the steels which were quenched and tempered. Figure 1 shows the processing and alloying strategy of the casing steels. Electric resistance welding (ERW) pipes were manufactured when the sheet metal was overlapped. The heat developed through a bias applied between the sheets causes the sheets to fuse together. A seamless pipe was manufactured using extrusion process. The testing steels can be divided into two groups with different alloying strategies. One group was alloyed with titanium–boron (Ti-B), whereas the other was alloyed with manganese–chromium–molybdenum (Mn-Cr-Mo).

**Table I** Chemical compositions of the casing steels (mass %)

| Steel | C | Mn | P | S | Si | Cr | Mo | Other |
|---|---|---|---|---|---|---|---|---|
| **ERW L80-B** | 0.24 | 0.98 | 0.007 | 0.0016 | 0.24 | 0.15 | 0.02 | Ca, Ti, B |
| **Seamless L80-B** | 0.25 | 1.13 | 0.014 | 0.0100 | 0.23 | 0.42 | 0.04 | Ca, Ti, B |
| **ERW L80-MnCr** | 0.25 | 1.34 | 0.007 | 0.0008 | 0.21 | 0.46 | 0.01 | Ca |
| **Seamless L80-Mo** | 0.28 | 1.10 | 0.010 | 0.0040 | 0.24 | 0.20 | 0.06 | Ca |
| **ERW L80-CrMo** | 0.24 | 1.12 | 0.012 | 0.0008 | 0.27 | 0.33 | 0.12 | Ca |
| **ERW L80-0.5Mo** | 0.25 | 0.69 | 0.007 | 0.0011 | 0.19 | 0.25 | 0.49 | Ca |

**Figure 1** The processing and alloying strategy of the casing steels, where ERW is electric resistance welding

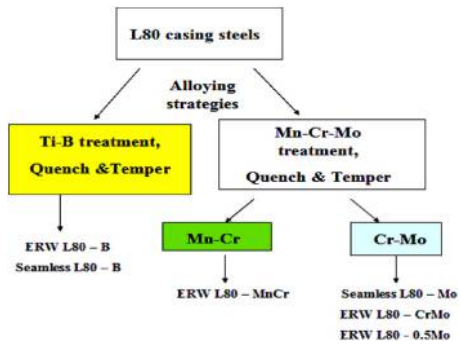


### 2.2 Microstructure observation and mechanical property test

To determine microstructures of the steels, the specimen was ground sequentially up to 1,200 grit silicon carbide paper, polished with 1 $\mu$m of diamond suspension and degreased with ethyl alcohol. It was then etched in 2 per cent Nital solution consisting of 2 ml nitric acid and 98 ml ethyl alcohol. The microstructures of the steels were observed using scanning electron microscope (SEM).

The actual yield strength (AYS) of steels was provided by Evraz Inc. NA. The Rockwell B hardness (HRB) was measured at three locations (e.g. 0°, 120° and 240°) around the shoulder of the round bar tensile specimens using a Wilson Rockwell B hardness meter with 100 kgf load.

### 2.3 Constant load tensile test

The constant load tensile tests were conducted to evaluate the SSC susceptibility of steels according to the Method A recommended by NACE Standard TM0177-2005 (2005). Smooth round bar tensile specimens with gauge diameter of 3.81 mm and gauge length of 25.4 mm were machined from the casing materials. The final surface finish of the test specimen was about 0.254 $\mu$m. The test solution consisted of 5.0 Wt.% sodium chloride and 0.5 Wt.% glacial acetic acid. Before the test, the solution was first bubbled with nitrogen to remove the oxygen and was then saturated with $H_2S$ gas. The specimen was installed in a proof ring testing device (supplied and calibrated by Cortest Inc.) on the uniaxial tensile testing machine, and 500 ml of solution was added into the device. Then, a constant load was applied to the specimen (The applied stress was 85 per cent of specified minimum yield strength). All the tests were carried out at room temperature (22°C) for the duration up to 720 h or until a complete breakage of the specimen. Two parallel runs for each steel were performed to confirm reproducibility of the results. Furthermore, the starting pH value of the test solution before $H_2S$ saturation should be in the range of 2.6-2.8, and the final one should be lower than 4.0 for the test to be valid. After the tests, the fracture

surfaces of the tensile specimens were examined by SEM and energy dispersive spectroscopy (EDS).

### 2.4 Characterizations of inclusion and carbide

Metallographic specimens with a surface area of 160 $mm^2$ were prepared from sections parallel to the longitudinal axis of the tube. Quantification of inclusions was performed using an optical microscope equipped with Clemex CIR 5.0 software. The inclusion population of 320 microscopic fields (0.5 $mm^2$/field) on each as-polished specimen was measured by Clemex CIR 5.0 software to obtain statistically relevant inclusion data.

The area fraction of different shapes of carbides in the microstructure was characterized by ImageJ 1.46 analysis software. The composition of carbide particles was identified using an SEM equipped with auger electron microscope (AES).

## 3. Results and discussion

### 3.1 Microstructure and mechanical property

Figure 2 shows the microstructures of the steels. In general, these microstructures were tempered martensite, and they consist of ferrite and carbides. The main difference between the microstructures is the distribution and shape of carbides. As seen in Figure 2(a) for the Ti-B steels, ERW L80-B and Seamless L80-B exhibit quite different microstructure. The microstructure of ERW L80-B mainly consists of ferrite and carbides. The carbides are mostly globular in shape and distributed inside the ferrite grains or along the grain boundaries. However, the microstructure of Seamless L80-B is composed of ferrite, carbides and islands of lamellar pearlite. Most of the carbides are clustered inside the lamellar structure and exhibit an elongated shape. Some are distributed inside the ferrite or along the grain boundaries. For the Mn-Cr-Mo steels in Figure 2(b), the microstructures of ERW L80-MnCr, ERW L80-CrMo and ERW L80-0.5Mo are similar to that of ERW L80-B, but the globular carbides in ERW L80-0.5Mo appear to be smaller and more dispersed throughout the structure. Notably, the segregation banding is present in ERW L80-MnCr [denoted by the yellow arrow in Figure 3(b)]. Furthermore, the microstructure of Seamless L80-Mo is quite similar to that of Seamless L80-B as mentioned earlier. The microstructures of the seamless materials indicate that Seamless L80-B and Seamless L80-Mo steels may not have been properly quenched during processing because the presence of lamellar pearlite is visible.

**Figure 2** Microstructures of the steels

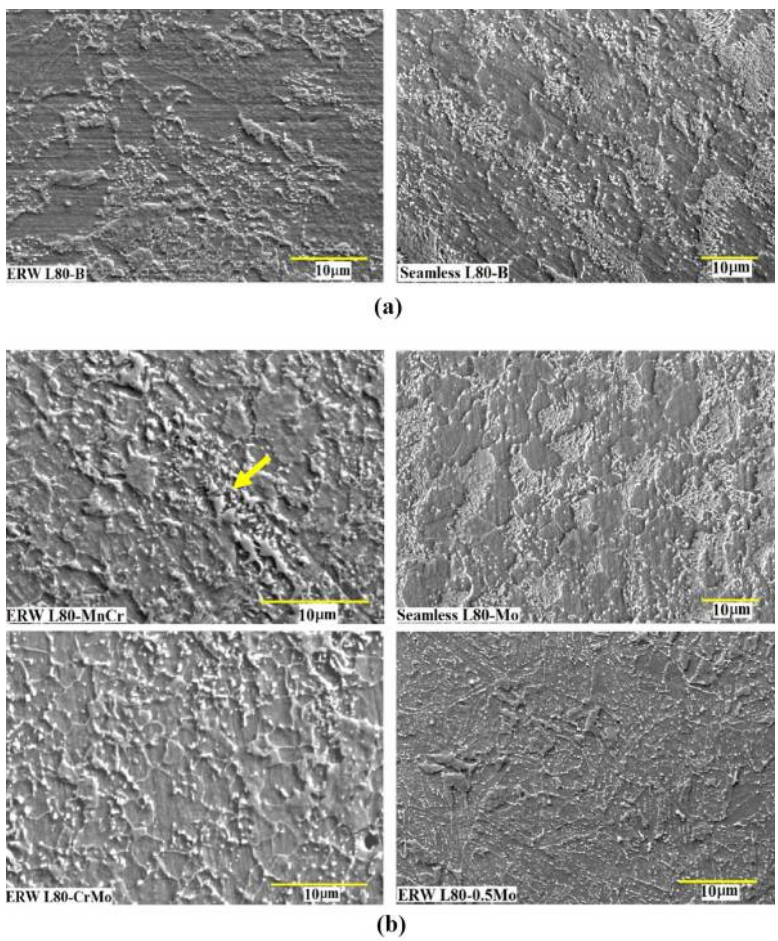


**Notes:** (a) Ti-B steel; (b) Mn-Cr-Mo steel

**Figure 3** Effect of yield strength on SSC resistance

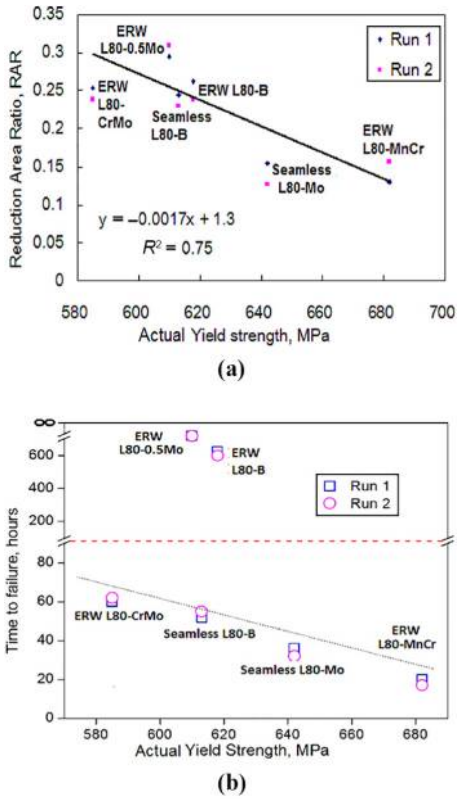


**Notes:** (a) *RAR* vs *AYS*; (b) time to failure vs *AYS*

Table II shows the AYS and Rockwell hardness values of the test steels. It can be seen that ERW L80-MnCr steel has the highest yield strength among all six steels, corresponding to the highest hardness, followed by Seamless L80-Mo. ERW L80-B, Seamless L80-B and ERW L80-0.5Mo steels all show negligent differences in yield strength (610-618 MPa) and hardness (89.1-89.8 HRB). However, ERW L80-CrMo steel has the minimal yield strength and hardness as compared to the other steels.

### 3.2 Evaluation of sulfide stress cracking susceptibility

Table III lists the results of SSC tests. ERW L80-0.5Mo steel is the only one that passes the720 h of test duration. The other steels either fail within 100 h or at around 400 h. ERW L80-0.5Mo and ERW L80-B steels are the two steels to surpass the 400 h margin before failure occurs. It is noteworthy that ERW L80-MnCr steel undergoes the SSC failure only within 20 h. Furthermore, the SSC susceptibility is evaluated based on time-to-failure data and loss in ductility. A parameter, *RAR*, is named reduction in area ratio and used to reflect the loss in ductility, which may be a more meaningful criterion for SSC evaluation. It can be calculated by the following equation:

$$RAR = \frac{RA_{\mathrm{H2S}}}{RA_{\mathrm{air}}} \quad (1)$$

where $RA_{\mathrm{H2S}}$ and $RA_{\mathrm{air}}$ are the reduction in area in $H_2S$ environment and in air, respectively. As shown in Figure 3, the time-to-failure or *RAR* has a general trend of decreasing with the increasing yield strength despite of the differences in alloying chemistries. Similar relationship for time-to-failure or *RAR* vs hardness can be found because of the positive relationship between the yield strength and hardness (Table III).

Figure 4 shows the fracture surface morphologies of the representative steels. For the steel with a higher *RAR* value (e.g. ERW L80-CrMo steel), the transgranular cracks are predominantly observed on the fracture surface [Figure 4(a)], indicative of a transgranular fracture mode. As shown in Figure 4(b), the transgranular and intergranular cracks simultaneously exist on the fracture surface of the steel with a lower *RAR* value (e.g. ERW L80-MnCr steel), indicating that its fracture is jointly dominated by transgranular and intergranular cracking.

The above results suggest that the high-yield strength can cause the significant decline of cracking resistance. As recommended by American Petroleum Institute [API specification 5CT (2005)], the fluctuation of yield strength of L80 casing steels should be lower than 15 ksi (e.g. in the range of 80-95 ksi or 552-655 MPa). Apparently, the yield strength of ERW L80-MnCr (682 MPa) exceeds the upper limit for L80 casing product in API specification 5CT, which may be one of the reasons for its higher susceptibility (Table III). However, although the yield strengths of other steels match the requirement of API specification, SSC failure still occurs in $H_2S$ environment except for ERW L80-0.5Mo steel. Especially, the steels with similar yield strengths, but different microstructures (e.g. ERW L80-B, Seamless L80-B and ERW L80-0.5Mo steels) show the different SSC resistance and failure time under the same conditions. Therefore, the SSC cracking behavior of steel does not solely depend on its mechanical properties, which is also related to the influence of alloying elements on the microstructure of steel (e.g. inclusion and carbide precipitation).

**Table II** Mechanical properties of the casing steels

| Steel | AYS (MPa) | Rockwell hardness (HRB) |
|---|---|---|
| ERW L80-B | 618 | 89.8 ± 2.4 |
| Seamless L80-B | 613 | 89.4 ± 4.8 |
| ERW L80-MnCr | 682 | 92.0 ± 1.9 |
| Seamless L80-Mo | 642 | 90.6 ± 4.2 |
| ERW L80-CrMo | 585 | 88.5 ± 4.9 |
| ERW L80-0.5Mo | 610 | 89.1 ± 1.7 |

### 3.3 Effect of inclusion on the sulfide stress cracking resistance of steel

Figure 5 correlates the total inclusion fraction with *RAR*. It can be seen that there is no obvious relationship between *RAR* and inclusion fraction for all steels. However, the *RAR* values of the steels within the same alloying group tend to decrease with the increase of inclusion fraction. Concurrently, the inclusion fraction is closely related to alloying composition of steels. As seen, ERW L80-0.5Mo steel has the lowest inclusion fraction among all the test steels, corresponding to the highest *RAR* value.

**Table III** Results of SSC proof ring test

| Steel | Initial/final pH | Result | Time to failure (hour) | *RAR* |
|---|---|---|---|---|
| **ERW L80-B** | 2.6/3.5 | Failure | 624 | 0.26 |
| | 2.7/3.5 | Failure | 600 | 0.24 |
| **Seamless L80-B** | 2.7/3.6 | Failure | 52 | 0.24 |
| | 2.7/3.6 | Failure | 60 | 0.23 |
| **ERW L80-MnCr** | 2.7/3.6 | Failure | 20 | 0.13 |
| | 2.6/3.6 | Failure | 17 | 0.16 |
| **Seamless L80-Mo** | 2.7/3.6 | Failure | 36 | 0.15 |
| | 2.7/3.6 | Failure | 32 | 0.12 |
| **ERW L80-CrMo** | 2.7/3.6 | Failure | 60 | 0.25 |
| | 2.7/3.6 | Failure | 62 | 0.24 |
| **ERW L80-0.5Mo** | 2.6/3.5 | No failure | >720 | 0.30 |
| | 2.7/3.6 | No failure | >720 | 0.31 |

**Figure 4** Fracture modes of steels in $H_2S$ environment

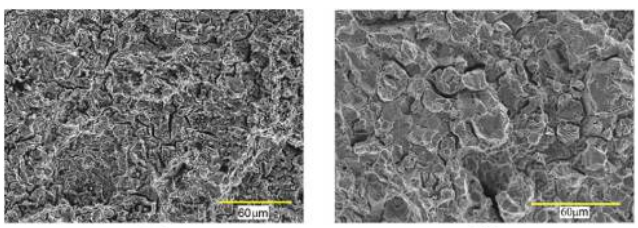


**Notes:** (a) Transgranular and intergranular mixed mode, ERW L80-MnCr (*RAR* = 0.13); (b) transgranular mode, ERW L80-CrMo (*RAR* = 0.25)

**Figure 5** Total inclusion fraction vs *RAR*

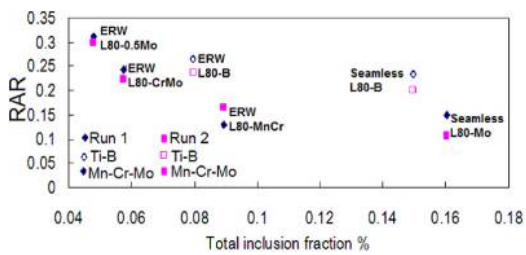


Figure 6 shows the area fractions of different shapes of inclusions in the steels. The fraction of globular inclusions (e.g. oxides) in the steels is remarkably higher than that of elongated inclusions (e.g. sulfide, alumina and silicate). The reason credited for this phenomenon is probably related to the addition of Ca in the steels. The added Ca contributes to the modification of inclusion shape and minimizes the formation of MnS inclusion. Because the elongated inclusion (e.g. soft and ductile MnS) can be modified into globular particles (e.g. CaS) by Ca, which cannot be elongated during rolling. This also helps to improve the cracking resistance of steel.

Figure 7 correlates the inclusion shape with *RAR* of different Mn-Cr-Mo and Ti-B steels. It can be seen that the increase in the fraction of elongated or globular inclusions corresponds to the significant decrease in *RAR* value of both Mn-Cr-Mo and

**Figure 6** Fraction of inclusions with different shapes in the steels

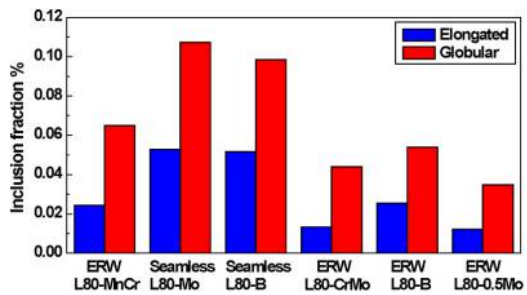


Ti-B alloyed steels, indicative of an adverse effect on the SSC resistance of steels. This is because the inclusions having a sharp interface with the matrix can act as stress raisers and provide easier crack paths for brittle crack propagation, which is an important factor governing the crack initiation stage. According to the slope of the linear relationship between *RAR* and inclusion shape per cent in Figure 7, the sensitivity of inclusion shape to SSC susceptibility can be determined, as listed in Table IV. Evidently, the elongated inclusions in Mn-Cr-Mo and Ti-B steels are more likely to affect SSC resistance adversely than globular inclusions.

Further inspection on the fracture surfaces of steels using SEM finds that the cracks are mainly originated from the elongated or oversized globular inclusions. Figure 8 clearly shows the initiation of crack at the elongated inclusions in Seamless L80-Mo and Seamless L80-B steels. EDS analysis suggests that the stringer inclusion (denoted by A) in Seamless L80-Mo steel mainly contains Mn and S elements [Figure 8(a)], indicating that it is the MnS inclusion, whereas that (denoted by B) in Seamless L80-B steel consists of Al, Si and O elements, corresponding to the Al-Si-O-enriched inclusion [Figure 8(b)]. As exhibited in Figure 9, the cracking initiation is also found at the globular oxide inclusion in Seamless L80-Mo steel. EDS analysis implies that the inclusion mainly consists of Ca, O and S elements. It is noteworthy that the size of globular oxide inclusion (denoted by B) is larger than 10 $\mu$m. The adverse effect of globular inclusion on SSC resistance may be because of the presence of oversized oxide (>10 $\mu$m) inclusions in the steels.

**Figure 7** Effect of inclusion shape on SSC resistance

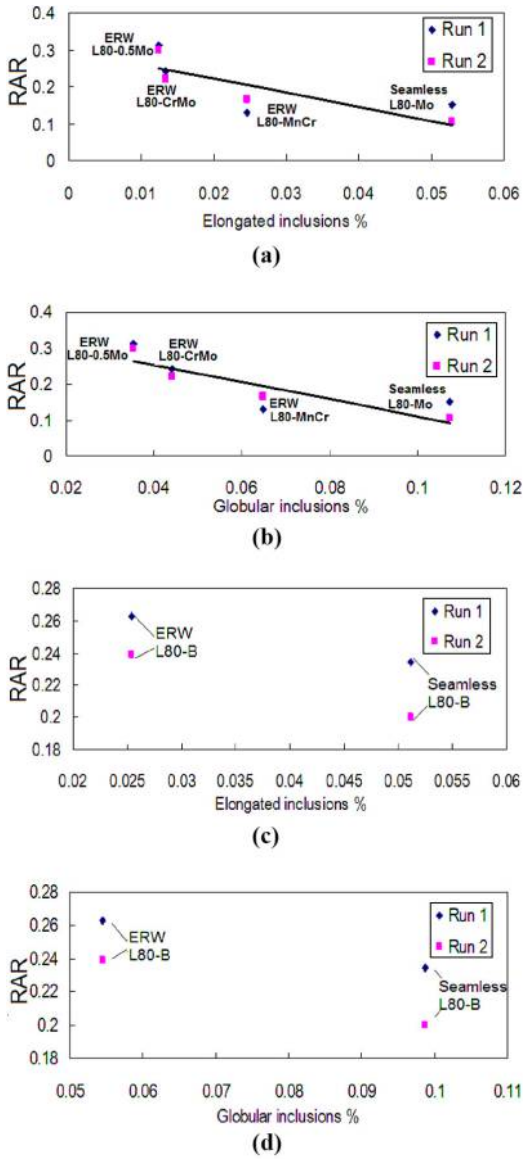


**Notes:** (a) Elongated inclusions vs *RAR* for Mn-Cr-Mo steels; (b) globular inclusions vs *RAR* for Mn-Cr-Mo steels; (c) elongated inclusions vs *RAR* for Ti-B steels; (d) Globular inclusions vs *RAR* for Ti-B steels

**Table IV** Sensitivity of inclusion shape to SSC susceptibility

| Steel | Elongated inclusion | Globular inclusion |
|---|---|---|
| **Mn-Cr-Mo** | −3.8 | −2.4 |
| **Ti-B** | −1.5 | −0.8 |

Furthermore, a closer examination on the steel surface finds obvious inclusion clusters in Seamless L80-Mo, Seamless L80-B, ERW L80-MnCr and ERW L80-CrMo steels, whereas no inclusion clusters are found in ERW L80-B and ERW L80-0.5Mo steels. The SEM morphologies of typical inclusion clusters in Seamless L80-B and ERW L80-MnCr with different alloying strategies, as the representatives, are shown in Figure 10. The inclusion clusters in Seamless L80-B steel are mainly Ca-Al-O-S, MnS and TiN inclusions [Figure 10(a)], whereas those in ERW L80-MnCr steel are Al-O inclusions [Figure 10(b)]. Especially, the microcracks were present around the Al-O inclusions in ERW L80-MnCr steel prior to the SSC test. Moreover, more inclusion clusters are found at the centerline of the steel thickness, which is probably generated by segregation during casting. These inclusion clusters with a dimension over 30 $\mu$m are the potential initiation sites of cracks, which can be further confirmed by the morphology observation on fracture surface. As seen in Figure 11, SSC of Seamless L80-B steel is evidently initiated from the Al-O and Ca-O inclusion clusters. Therefore, the presence of inclusion cluster in the steel can be reasonably believed to be quite detrimental for the SSC resistance of steel, which can significantly increase the SSC susceptibility of steel. This is quite consistent with the results of SSC tests in Table III. As seen, ERW L80-B or ERW L80-0.5Mo steel without obvious inclusion clusters needs a longer time to failure (>600 h) or no failure at all in the test duration of 720 h as compared to the steels with inclusion clusters.

### 3.4 Effect of carbide on the sulfide stress cracking resistance of steel

ERW L80-0.5Mo, Seamless L80-Mo, ERW L80-B and Seamless L80-B steels with different alloying strategies, as the representatives, were used for the characterization of carbides. A closer observation on the type of carbides in the steels using AES confirms that the carbides in the steels are mainly identified as iron carbides. However, the molybdenum carbide with a globular shape can also be found in ERW L80-0.5Mo steel in addition to iron carbides, as confirmed by the SEM observation and AES analysis in Figure 12. The correlations between the fraction of carbide with different shapes and *RAR* are shown in Figure 13. It can be determined that the low fraction of elongated carbides has the positive effect on the cracking resistance. Although the high fraction of globular carbides is present in the steels (e.g. ERW L80-0.5Mo and ERW L80-B), the fractions of inclusions especially the elongated inclusions are very low, and the elongated inclusion has a larger impact on the cracking resistance as shown in Figure 7. Therefore, the globular carbide in the steel might reduce the negative effect on the cracking resistance, but the effect of globular carbide may be shielded by the elongated inclusion to some extent. The sensitivity of carbide shape on SSC resistance can be calculated from the slope of the linear relationship between *RAR* and carbide shape per cent in Figure 13. The sensitivity of elongated carbide is about −0.0078, while that of globular carbide is about 0.036. More specifically, the SSC resistance of steel is more sensitive to the change in the content of elongated carbide.

As compared to the sensitivities of inclusions in Table IV, it is apparent that the inclusions have a larger effect on SSC resistance than carbides. Evidently, the high cracking resistance of the steels (e.g. ERW L80-0.5Mo and ERW L80-B) should be mainly related to the low content of inclusions. Fracture surface examination also confirms that the inclusions are the

**Figure 8** SEM morphology of crack initiation at elongated inclusions and the EDS analyses of the corresponding inclusions

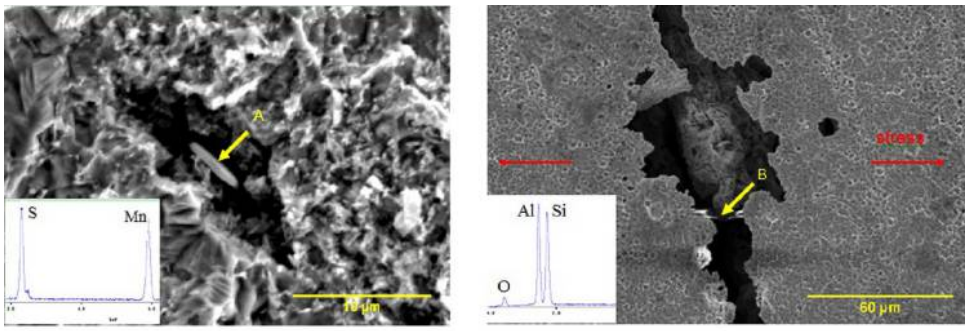


(a) (b)

**Notes:** (a) MnS in Seamless L80-Mo; (b) Al-Si-O-enriched inclusions in Seamless L80-B

**Figure 9** SEM morphology of crack initiation at large globular inclusions and the EDS analysis of the corresponding inclusion in Seamless L80-Mo steel

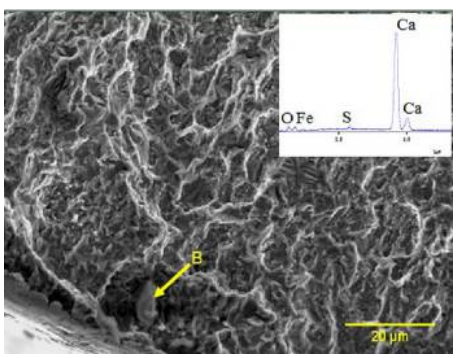


**Figure 10** SEM images of inclusions clustering at centerline locations in different steels

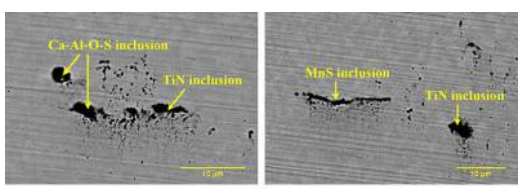


(a)

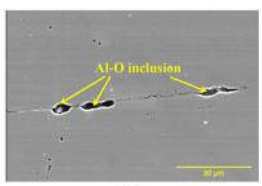


(b)

**Notes:** (a) Seamless L80-B steel; (b) ERW L80-MnCr steel

**Figure 11** Crack nucleation at inclusion cluster enriched with Al-O and Ca-O in Seamless L80-B steel

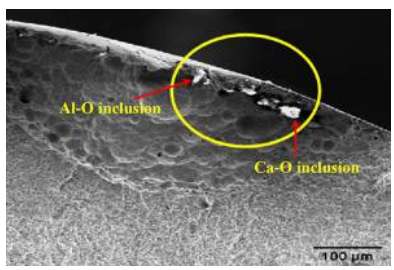


critical crack nucleation sites for SSC (Figures 8-11). However, this does not mean that the carbides have no influence on the SSC behavior. A good microstructure should be able to stop the propagation of crack once it is initiated. The distribution and morphology of carbides in the microstructure are believed to play an important role in SSC propagation. Comparisons of the microstructure of ERW L80-0.5Mo with other steels (Figure 2) suggest that a uniform microstructure with fine globular carbides can improve SSC resistance (Table III). This may be because of the high density and uniform distribution of carbide traps in the microstructure, which minimizes the diffusion of mobile hydrogen to susceptible regions (e.g. inclusions or an existing crack initiated from inclusion) to cause embrittlement. Inversely, the clusters of elongated carbides in the microstructure of steel (e.g. Seamless L80-B steel and Seamless L80-Mo steel) act as the large hydrogen accumulation sites and provide ready crack paths for crack propagation. As shown in Figure 14, transgranular HIC crack nucleated from the pearlite colonies (indicated by the circle in the figure) and propagated through the matrix in Seamless L80-Mo steel.

## 4. Conclusions

- Among the steels investigated in this study, ERW L80-0.5Mo steel has the appropriate mechanical properties, uniform microstructure with fine globular carbide and

**Figure 12** SEM image and auger spectra of globular molybdenum carbides in ERW L80-0.5Mo steel

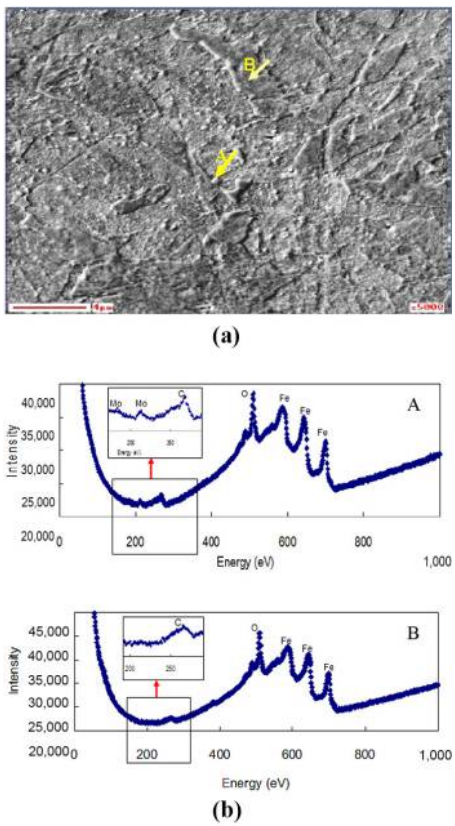


**Notes:** (a) SEM image: globular molybdenum carbide denoted by A and background for comparison denoted by B; (b) Auger spectra of the regions denoted by A and B in (a)

**Figure 13** Effect of carbide shape on the SSC resistance

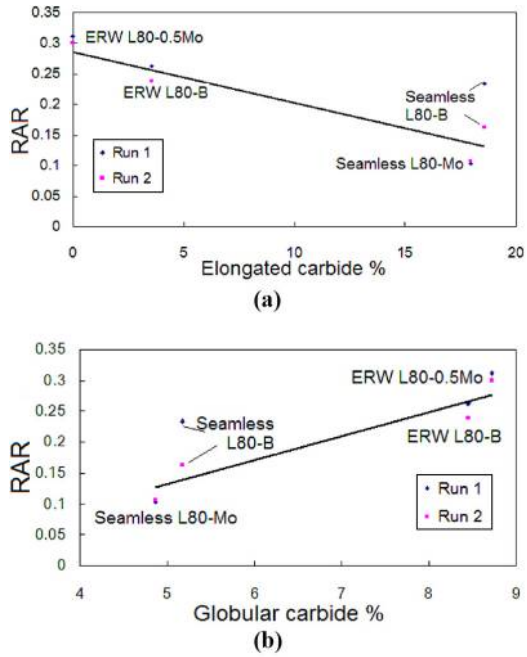


**Notes:** (a) Elongated carbides vs *RAR*; (b) globular carbide vs *RAR*

**Figure 14** Transgranular HIC initiated from the pearlite colonies (indicated by the circle) and propagated through the matrix in Seamless L80-Mo

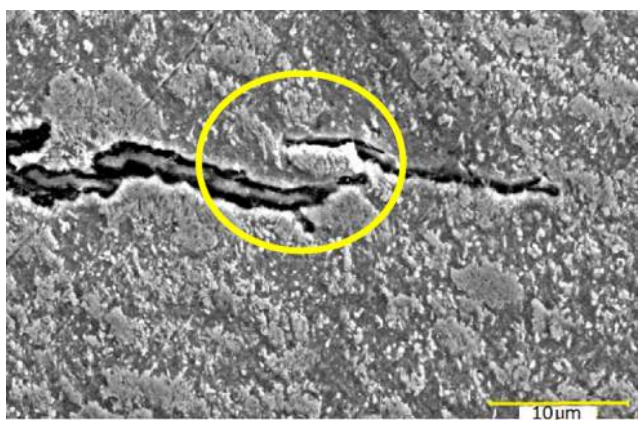


lowest inclusion content, corresponding to the highest SSC resistance.

- The SSC resistance of L80 casing steel generally decreases with the increase of its yield strength (or hardness). For the steel of lower resistance to cracking, the combination of transgranular and intergranular fracture is the dominant cracking mode, whereas the fracture of the steel with higher cracking resistance is mainly controlled by the transgranular mode.
- SSC is more sensitive to inclusions than carbides because the inclusions are the critical nucleation sites of cracks. Compared to globular inclusions, SSC is readily initiated from the elongated inclusions (e.g. Mn-S and Al-Si-O) and large oxide inclusions (e.g. Ca-O-S) with sizes over 10 $\mu$m, especially the inclusion clusters with sizes over 30 $\mu$m.
- The increased content of elongated carbide reduces the SSC resistance of steel. However, the globular carbides can reduce the negative effect on the SSC resistance. Especially, a uniform microstructure with fine globular carbides contributes to an improvement in SSC resistance through precluding the cracking propagation.

## References

API Specification 5CT (2005), *Specification for Casing and Tubing*, American Petroleum Institute, Washington, DC.

Al-Mansour, M., Alfantazi, A.M. and El-boujdaini, M. (2009), "Sulfide stress cracking resistance of API-X100 high strength low alloy steel", *Materials & Design*, Vol. 30 No. 10, pp. 4088-4094.

Beidokhti, B., Dolati, A. and Koukabi, A.H. (2009), "Effects of alloying elements and microstructure on the susceptibility of the welded HSLA steel to hydrogen-induced cracking and sulfide stress cracking", *Materials Science and Engineering: A*, Vol. 507 Nos 1/2, pp. 167-173.

Bai, P.P., Zhao, H., Zheng, S.Q. and Chen, C.F. (2015), "Initiation and developmental stages of steel corrosion in wet $H_2S$ environments", *Corrosion Science*, Vol. 93, pp. 109-119.

Choi, Y.S., Nešić, S. and Ling, S. (2011), "Effect of $H_2S$ and $CO_2$ corrosion of carbon steel in acidic solutions", *Electrochimica Acta*, Vol. 56 No. 4, pp. 1752-1760.

Ding, J.H., Zhang, L., Lu, M.X., Wang, J., Wen, Z.B. and Hao, W.H. (2014), "The electrochemical behaviour of 316L austenitic stainless steel in $Cl^-$ containing environment under different $H_2S$ partial pressures", *Applied Surface Science*, Vol. 289, pp. 33-41.

Elboujdaini, M. (2011), "Hydrogen induced cracking and sulfide stress cracking", in Revie, R.W. (Ed.), *Uhlig's Corrosion Handbook*, John Wiley & Sons, Hoboken, NJ, pp. 183-192.

Golovanenko, S.A., Zikeev, V.N., Serebryanaya, E.B. and Popova, L.V. (1978), "Effect of alloying elements and structure on the resistance of structural steels to hydrogen embrittlement", *Metal Science and Heat Treatment*, Vol. 20 No. 1, pp. 3-14.

Guo, S.Q., Xu, L.N., Zhang, L., Chang, W. and Lu, M.X. (2012), "Corrosion of alloy steels containing 2% chromium in $CO_2$ environments", *Corrosion Science*, Vol. 63, pp. 246-258.

He, W., Knudsen, O.Ø. and Diplas, S. (2009), "Corrosion of stainless steel 316L in simulated formation water environment with $CO_2$-$H_2S$-Cl", *Corrosion Science*, Vol. 51 No. 12, pp. 2811-2819.

Jin, T.Y., Liu, Z.Y. and Cheng, Y.F. (2010), "Effect of non-metallic inclusions on hydrogen-induced cracking of API5L X100 steel", *International Journal of Hydrogen Energy*, Vol. 35 No. 15, pp. 8014-8021.

Koh, S.U., Yang, B.Y. and Kim, K.Y. (2004), "Effect of alloying elements on the susceptibility to sulfide stress cracking of line pipe steels", *Corrosion*, Vol. 60 No. 3, pp. 262-274.

Kang, H.J., Yoo, J.S., Park, J.T., Ahn, S.T., Kang, N. and Cho, K.M. (2012), "Effect of nano-carbide formation on hydrogen-delayed fracture for quenching and tempering steels during high-frequency induction heat treatment", *Materials Science and Engineering: A*, Vol. 543, pp. 6-11.

López, D.A., Pérez, T. and Simison, S.N. (2003), "The influence of microstructure and chemical composition of carbon and low alloy steels in $CO_2$ corrosion", *Materials & Design*, Vol. 24 No. 8, pp. 561-575.

Lei, X.W., Wang, H.Y., Mao, F.X., Zhang, J.P., Zhao, M.F., Fu, A.Q., Feng, Y.R. and Macdonald, D.D. (2018), "Electrochemical behaviour of martensitic stainless steel after immersion in a $H_2S$-saturated solution", *Corrosion Science*, Vol. 131, pp. 164-173.

NACE Standard TM0177-2005 (2005), *Standard Test Method: Laboratory Testing of Metals for Resistance to Sulfide Stress Cracking and Stress Corrosion Cracking in H2S Environments*, NACE International, Houston, TX.

Peñalva, G.A.I., Legarda, F., Esteban, G.A. and Riccardi, B. (2012), "Interaction of copper alloys with hydrogen", in Collini, L. (Ed.), *Copper Alloys - Early Applications and Current Performance - Enhancing Processes*, InTech, Croatia, pp. 31-48.

Sponseller, D.L., Garber, R. and Straatmann, J.A. (1983), "Effect of microstructure on sulfide-stress-cracking resistance of high-strength casing steels", in Abrams, H., Hood, J. and Seth, B. (Ed.), *MiCon 82: Optimization of Processing, Properties, and Service Performance through Microstructural Control*, ASTM International, West Conshohocken, PA, pp. 172-204.

Sun, J.B., Sun, C., Lin, X.Q., Cheng, X.K. and Liu, H.F. (2016), "Effect of chromium on corrosion behaviour of P110 steels in $CO_2$-$H_2S$ environment with high pressure and high temperature", *Materials*, Vol. 9 No. 3, p. 200.

Sui, Y.Y., Sun, C., Sun, J.B., Pu, B.L., Ren, W. and Zhao, W.M. (2017), "Stability of an electrodeposited nanocrystalline Ni-based alloy coating in oil and gas wells with the coexistence of $H_2S$ and $CO_2$", *Materials*, Vol. 10 No. 6, p. 632.

Sun, C., Li, J.K., Shuang, S., Zeng, H.B. and Luo, J.-L. (2018), "Effect of defect on corrosion behaviour of electroless Ni-P coating in $CO_2$-saturated NaCl solution", *Corrosion Science*, Vol. 134, pp. 23-37.

Venegas, V., Caleyo, F., González, J.L., Baudin, T., Hallen, J. M. and Penelle, R. (2005), "EBSD study of hydrogen-induced cracking in API-5L-X46 pipeline steel", *Scripta Materialia*, Vol. 52 No. 2, pp. 147-152.

Wu, Q.L., Zhang, Z.H., Dong, X.M. and Yang, J.Q. (2013), "Corrosion behavior of low-alloy steel containing 1% chromium in $CO_2$ environments", *Corrosion Science*, Vol. 75, pp. 400-408.

Zhang, G.A., Zeng, Y., Guo, X.P., Jiang, F., Shi, D.Y. and Chen, Z.Y. (2012), "Electrochemical corrosion behaviour of carbon steel under dynamic high pressure $H_2S/CO_2$ environment", *Corrosion Science*, Vol. 65, pp. 37-47.

Zhou, C.S., Zheng, S.Q., Chen, C.F. and Lu, G.W. (2013), "The effect of the partial pressure of $H_2S$ on the permeation of hydrogen in low carbon pipeline steel", *Corrosion Science*, Vol. 67, pp. 184-192.

Zheng, Y.G., Brown, B. and Nešić, S. (2014), "Electrochemical study and modeling of $H_2S$ corrosion of mild steel", *Corrosion*, Vol. 70 No. 4, pp. 351-365.

## Corresponding author

**Jing-Li Luo** can be contacted at: jingli.luo@ualberta.ca and **Hani Henein** can be contacted at: hhenein@ualberta.ca